Liquid Crystals
Publication details, including instructions for authors and subscription information:
http://www.informaworld.com/smpp/title~content=t713926090

Computer simulations of the interactions between liquid crystal molecules and polymer surfaces III. Use of pseudopotentials to represent the surface

D. R. Binger; S. Hanna

Online publication date: 06 August 2010

To cite this Article Binger, D. R. and Hanna, S.(2001) 'Computer simulations of the interactions between liquid crystal molecules and polymer surfaces III. Use of pseudopotentials to represent the surface', Liquid Crystals, 28: 8, 1215 — 1234
To link to this Article: DOI: 10.1080/02678290110052412
URL: http://dx.doi.org/10.1080/02678290110052412

LIQUID CRYSTALS, 2001, VOL. 28, NO. 8, 1215–1234

Computer simulations of the interactions between liquid crystal molecules and polymer surfaces III. Use of pseudopotentials to represent the surface

D. R. BINGER and S. HANNA*

H. H. Wills Physics Laboratory, University of Bristol, Tyndall Avenue, Bristol BS8 1TL, UK

(*Received 30 November 2000; in final form 16 February 2001; accepted 26 February 2001*)

Results are presented from atomistic computer simulations of single molecules of the liquid crystals 4-*n*-octyl-4′-cyanobiphenyl and 4-*n*-heptyl-2-fluorophenyl 4-octyloxybiphenyl-4′-carboxylate in contact with crystalline polymeric surfaces. The simulations were performed as part of a study of the nature of the alignment interactions in liquid crystal displays and other devices. In contrast to previous atomistic simulations of this type, the crystalline polymer surface was represented by a pseudopotential, effectively replacing the parallel array of polymer chains with a periodic corrugation. The use of a pseudopotential has two main advantages. Firstly, it allows an exploration of the general principles behind liquid crystal alignment on crystalline surfaces, free from the obscuring effect of specific chemical interactions. Secondly, it permits a significant saving in computer time compared with using a surface constructed from explicit atom-pair potentials. In the present work, the aligning capabilities of two simple sinusoidal pseudopotential functions were tested. In each case the wavelength and amplitude of the surface corrugations were varied. It was found that the degree of orientational order of liquid crystal molecules in contact with the surfaces increased with increasing amplitude and decreasing wavelength of the corrugations. Aspects of the two potentials were then combined to produce a pseudopotential designed to represent specific polymeric crystal surfaces. In this case, the (1 0 0) and (1 1 0) faces of polyethylene were modelled. Comparisons with earlier simulations employing atomistic surfaces indicate a good agreement between the orientation functions produced by the two methods. However, the pseudopotential approach uses significantly less computer time, allowing a more reliable determination of orientation within a given timescale.

1. Introduction

The successful operation of liquid crystal display devices is dependent on the correct functioning of an alignment layer, which is usually made of polymer and which ensures that the liquid crystal molecules are uniformly oriented in the vicinity of the cell surface. The molecular organization at the interface is not clearly understood in either the liquid crystal or the polymer film, because most experimental structural techniques are only able to probe the bulk of the material. Even surface sensitive techniques such as second harmonic generation, while giving the average orientation of the liquid crystal monolayer closest to the cell surface [1, 2], give no direct information about the molecular organization or packing within that monolayer. Also, studies of liquid crystal monolayers, using the scanning tunnelling microscope, have only been able to elucidate the molecular packing which is specific to graphite surfaces, rather than polymeric alignment layers [3–6]. However, it is now generally accepted that one possible alignment mechanism is that the polymer chains in the surface layer of the polymer become oriented due to friction during the fabrication process, and that the liquid crystal molecules align through local, molecular level, interactions with the polymer chains [2, 7, 8].

Although there has been a large body of research on the simulation of bulk liquid crystal phases [9], to date there have been relatively few computer simulation studies of liquid crystals interacting with alignment layers. Recently, several groups have reported the use of Gay–Berne models to simulate the behaviour of liquid crystals in the vicinity of different types of wall [10–16]. Such simulations are extremely valuable for demonstrating molecular ordering at interfaces and the possible origins of molecular pretilt. Rather fewer atomistic simulations of liquid crystal interfaces have been published,

*Author for correspondence; e-mail: s.hanna@bristol.ac.uk

Liquid Crystals ISSN 0267-8292 print/ISSN 1366-5855 online © 2001 Taylor & Francis Ltd
http://www.tandf.co.uk/journals
DOI: 10.1080/02678290110052412

and the computational expense of such simulations means that, in general, only very small systems of molecules have been studied. For example, Cleaver *et al.* [17, 18] and Yoneya and Iwakabe [19] have considered the interactions between 4-*n*-octyl-4′-cyanobiphenyl (8CB) and a graphite substrate, while Yoneya and Iwakabe have also looked at interactions of 8CB with close packed layers of polyimide and polyamide molecules [20, 21]. In the latter case, it was found that the liquid crystal molecules preferentially aligned parallel to the axes of the polymer molecules and that the mean orientational order parameter, P_2, decreased if the number density of polymer molecules in the alignment layer was reduced.

More recently, Doerr and Taylor [22, 23] have performed simulations of 4-*n*-pentyl-4′-cyanobiphenyl (5CB) at an amorphous polyethylene surface. Although the size and time scale of the simulations were limited, they showed a clear tendency towards homeotropic alignment. Similarly, Patnaik and Pachter [24] have shown that amorphous or homeotropic configurations of 5CB are energetically favoured over planar configurations at amorphous polyacrylate surfaces.

In a number of previous publications [25–27], we have used computer simulations to examine the behaviour of two liquid crystal molecules, 8CB and MBF (see figure 1), in contact with a variety of crystalline polymeric surfaces. Our studies were restricted to crystalline surfaces for several reasons. Firstly, it is known that chain orientation and extension, which would occur during the rubbing process, promote polymer crystallization [28]. Secondly, it is generally observed that semi-crystalline polymers align liquid crystals more effectively than glassy polymers [7, 29]. Finally, a technical point is that crystalline surfaces are more easily specified than amorphous surfaces. The present paper continues the study of crystalline surfaces, although work is in hand to extend the methods to amorphous materials.

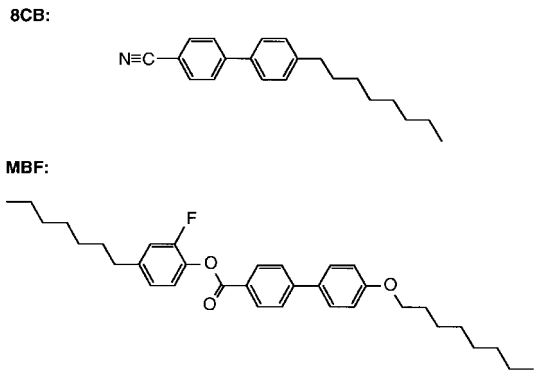

Figure 1. The structures of the liquid crystal molecules 4-*n*-octyl-4′-cyanobiphenyl (8CB) and 4-*n*-heptyl-2-fluorophenyl 4-octyloxybiphenyl-4′-carboxylate (MBF).

In our previous simulations, only planar configurations of the liquid crystal molecules were examined on the polymer substrates. The main finding was that the liquid crystal alignment depended on the geometry of both the polymer and the liquid crystal molecule, with the topography of the polymer surface being of paramount importance. It was found that polymer crystal faces with clearly defined molecular level corrugations produced good alignment, and that the quality of alignment depended on both the spacing and the depth of those corrugations. For example, the deep corrugations formed by the backbones of adjacent polymer chains on the (1 0 0) surface of poly(vinyl alcohol) produced a more clearly defined alignment than the relatively shallow corrugations on the (1 0 0) or (1 1 0) faces of polyethylene. Electrostatic interactions were found to be only of secondary importance in determining alignment preferences.

In order to make the aligning effect of the corrugations more quantifiable, we have replaced the selection of polymer surfaces used in previous papers with a simple pseudopotential energy function. The pseudopotential allows us to look at the influence of generic surfaces on molecular alignment, without having to consider specific molecular detail. Using the pseudopotential, we are able to explore various geometric aspects of polymer surfaces which are required in order to produce good liquid crystal alignment. A fortunate biproduct of the use of the pseudopotential is that the molecular dynamics simulations require less computer time than those involving explicit surface atoms. This, in turn, means that it is possible to perform simulations over a longer time scale than previously, and gather more reliable statistics for the orientation functions measured.

In this paper, we describe the use of two simple sinusoidal pseudopotential energy functions to represent the polymer surface. In each case we examine the trajectory of a simple rod-like liquid crystal molecule (8CB) in contact with a range of surfaces with varying corrugation wavelengths and amplitudes, with a view to quantifying the orienting power of each surface. We also show how the pseudopotentials may be combined to represent a real polymer crystal surface, and comparisons are drawn with earlier simulation work using atomistic potentials for both 8CB and MBF. A further paper will demonstrate the use of the realistic pseudopotential in large scale atomistic simulations of the interfacial region between a polymer alignment layer and a bulk liquid crystal phase [30].

2. Background

The use of pseudopotentials for representing crystalline surfaces has been demonstrated previously by Steele [31], and applied to interactions with gaseous molecules.

The approach used was to represent the surface potential by a two-dimensional Fourier series:

$$u(\mathbf{r}) = \sum_{g}\sum_{\alpha} w_g(z_\alpha)\exp(\mathrm{i}\mathbf{g}\ \ \boldsymbol{\tau}) \tag{1}$$

where $\boldsymbol{\tau}$ is a translation vector in the plane of the substrate, $\mathbf{g}$ is a reciprocal lattice vector and $w_g(z_\alpha)$ is the Fourier coefficient for the αth plane of surface atoms located at a distance z_α from the gas atom. In the case of the Lennard–Jones 12-6 potential, the analysis gave:

$$u(\mathbf{r}) = \frac{2\pi E_{gs}}{a_s}\sum_{\alpha}\left\{q\left(\frac{2\sigma_{gs}^{12}}{5z_\alpha^{10}} - \frac{\sigma_{gs}^{6}}{z_\alpha^{4}}\right) + \sum_{g\neq 0}\sum_{k=1}^{q}\exp(\mathrm{i}\mathbf{g}\ \ [\mathbf{m}_k + \boldsymbol{\tau}]) \times\left[\frac{\sigma_{gs}^{12}}{30}\left(\frac{g}{2z_\alpha}\right)^5 K_5(gz_\alpha) - 2\sigma_{gs}^{6}\left(\frac{g}{2z_\alpha}\right)^2 K_2(gz_\alpha)\right]\right\} \tag{2}$$

where a_s is the cross-sectional area of the unit cell in the crystal surface, q is the total number of atoms in the unit cell, and $\mathbf{m}_k$ is the position vector of the kth atom in the unit cell. σ_{gs} is the equilibrium separation and E_{gs} the potential well depth between a surface atom and a gas atom. Finally, K_n is the nth order modified Bessel function of the second kind.

The Steele equation provides an accurate representation of the surface, but for any real application the Fourier sum needs to be truncated. However, if the substrate possesses symmetry, the expression may be simplified, and results in a rapid method for calculating the surface potential. The Steele equation and variations on it have been used widely in studies of adsorption of small molecules on graphite. Particular examples include adsorption of N_2 molecules [32, 33] and adsorption of the liquid crystal molecule 8CB [13].

In the present application, which involves liquid crystal molecules on polymeric substrates, our previous analyses [25–27] suggest that the behaviour of the liquid crystal will be dominated by short range interactions with a topologically anisotropic substrate. In such circumstances, it is found that a large number of terms is required in the Steele equation for an accurate representation of the polymer surface. This is a particular problem because of the comparatively large number of atoms in a typical polymeric unit cell. For example, there are 12 atoms in the unit cell of polyethylene and 152 in the unit cell of Nylon 6, compared with only four in graphite. Bearing in mind, also, the fact that the van der Waals interactions are normally truncated at *c.* 8.5 Å, the overall result is that there may be little speed advantage in the use of the Steele equation compared with a direct summation of the Lennard–Jones potential. For this reason, we decided that a simpler approach was required, in which, rather than attempting to reproduce the polymer surface exactly, only its most important feature, i.e. the corrugation created by adjacent polymer chains, would be modelled. The approach is described below.

3. The cosine pseudopotential

The requirements of the polymer pseudopotential are that it should act as a barrier to the liquid crystal molecules, and that it should be modulated in some way to represent the polymer chain corrugations. In all that follows we will assume that the surface lies in the *xy*-plane, with the polymer chain axis parallel to the *y*-axis. We define the *corrugation direction* as being parallel to the polymer chain axis. In all of the functions derived, the potential energy is independent of the *y*-coordinate.

The barrier part of the pseudopotential was formed by considering a standard Lennard–Jones 12-6 potential:

$$u(r) = E\left[\left(\frac{\sigma}{r}\right)^{12} - 2\left(\frac{\sigma}{r}\right)^{6}\right] \tag{3}$$

where E is the potential well depth, and σ the equilibrium separation of a probe atom from an atom in the substrate. The surface was considered to contain a uniform density of atoms, and equation (3) was integrated to include the interactions between a probe atom at height z above the surface and all of the atoms in the half space below the surface, to give:

$$U(z) = \frac{n\pi E\sigma^3}{45}\left[\left(\frac{\sigma}{z}\right)^9 - 15\left(\frac{\sigma}{z}\right)^3\right]. \tag{4}$$

In equation (4), n is the number density of atoms in the substrate. The surface corrugation was then introduced by modulating either the well depth E or the equilibrium separation σ with the aim of producing surfaces in which the corrugations were either purely due to variations in potential well depth, or purely due to topography. The extent to which this was achieved is shown below.

3.1. *E-modulated cosine pseudopotential*

In the first method of modulating the surface, the modulation was obtained by replacing E in equation (4) with:

$$E(x) = E_0 + \frac{\Delta E}{2}[1 + \cos(2\pi x/\lambda)] \tag{5}$$

where the wavelength of the corrugation is λ. The potential energy is then written as:

$$U(x, z) = \frac{n\pi E(x)\sigma^3}{45}\left[\left(\frac{\sigma}{z}\right)^9 - 15\left(\frac{\sigma}{z}\right)^3\right]. \tag{6}$$

This function is shown as a contour plot in figure 2(*a*). It can be seen that the equation represents a hard wall adjacent to a periodic array of potential wells. The potential wells are linear, i.e. they are extended parallel to the *y*-axis. The lowest energy parts of the potential wells are located at a distance $\sigma/5^{1/6}$ from the wall. The variation in energy found on traversing the surface at this height is $(2\sqrt{5}/9)n\pi\sigma^3\Delta E$.

3.2. *σ-Modulated cosine pseudopotential*

The second method of modulating the surface was to replace σ in equation (4) with:

$$\sigma(x) = \sigma_0 + \frac{\Delta\sigma}{2}[1 + \cos(2\pi x/\lambda)]. \tag{7}$$

In this case, the resulting potential energy function represents a variation in the position of the potential well relative to the surface. The distance of the well from the wall varies by $\Delta\sigma/5^{1/6}$. Although the well depth of the Lennard–Jones potential given in equation (3) is independent of σ, that of the integrated potential is not, and is given by:

$$U_0(x) = -\frac{2\sqrt{5}}{9}n\pi E\sigma(x)^3. \tag{8}$$

Unfortunately, this means that the equilibrium potential energy is lower at the peaks of the corrugations than at the troughs. This inconsistency is corrected for by scaling the potential energy function by $[\sigma_0/\sigma(x)]^3$, so that the equilibrium potential energy is independent of the position across the corrugation at which it is measured. The final σ-modulated potential energy function is given by:

$$U(x, z) = \frac{n\pi E\sigma_0^3}{45}\left[\left(\frac{\sigma(x)}{z}\right)^9 - 15\left(\frac{\sigma(x)}{z}\right)^3\right] \tag{9}$$

and is shown as a contour plot in figure 2(*b*). It is clear that equation (9) represents a corrugated wall adjacent to a similarly corrugated potential well.

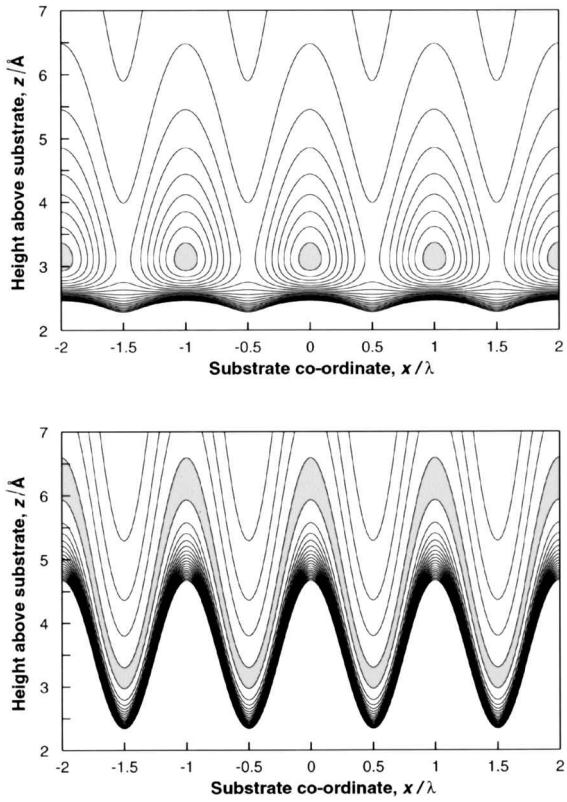

Figure 2. Graph showing potential energy contours calculated for (*a*) the *E*-modulated cosine pseudopotential of equation (6) and (*b*) the σ-modulated cosine pseudopotential of equation (9). In (*a*) the modulation depth is $\Delta E/E_0 = 3$, while in (*b*) the modulation depth is $\Delta\sigma/\sigma_0 = 1$. The positions of the potential energy minima are indicated by shading, and only negative potential energy contours are shown. The energy contours are shown in steps of $2E_0$ in (*a*) and E_0 in (*b*); in both cases, $E_0 = 0.83\,\text{kJ mol}^{-1}$ and $\sigma_0 = 4.0677$ Å

4. The polyethylene (PE) pseudopotential

The method described above for introducing periodic variations in the depth or position of the Lennard–Jones potential well, raises the possibility that more complex modulations could be introduced. For example, the variations in *E* or σ could be represented by a Fourier series, rather than a single cosine function. However, it is clear that modulations in both *E* and σ will be required in order to obtain a good fit to, say, a crystalline face of polyethylene (PE). An alternative energy expression, which satisfies this requirement, will now be derived.

The faces of any molecular crystal will not be smooth on an Ångstrom scale, and this will introduce some uncertainty over the precise location of the wall, relative to an arbitrary origin. Thus, we rewrite equation (4), allowing the origin to be offset by η in the *z* direction:

$$U(z) = \frac{n\pi E\sigma^3}{45}\left[\left(\frac{\sigma}{z-\eta}\right)^9 - 15\left(\frac{\sigma}{z-\eta}\right)^3\right]. \tag{10}$$

The position of minimum potential energy, ζ, will be given by:

$$\zeta = 5^{1/6} + \eta \tag{11}$$

at which point, the minimum potential energy, ϕ, will be:

$$\phi = -\frac{10n\pi E}{9}(\zeta - \eta)^3. \tag{12}$$

Equations (11) and (12) are used to eliminate σ and E from equation (10), yielding:

$$U(x,z) = -\frac{\phi(x)}{2}\left[\left(\frac{\zeta(x)-\eta(x)}{z-\eta(x)}\right)^9 - 3\left(\frac{\zeta(x)-\eta(x)}{z-\eta(x)}\right)^3\right] \quad (13)$$

where now ϕ, ζ and η are taken to be functions of x, which will need to be determined for any particular crystal surface. No potential energy variation is permitted in the y-direction, i.e. parallel to the polymer chain axis.

$\phi(x)$, $\zeta(x)$ and $\eta(x)$ were obtained by fitting equation (13) to the results of explicit atom-pair calculations of the potential energy above slabs of crystalline PE. The atomic coordinates and unit cell parameters of PE were taken from the literature [34] and the Dreiding 2 force-field was used with the CH_2 groups represented by united atoms [35]. A Lennard–Jones 12-6 potential was used, with $E = 0.71\,\mathrm{kJ\,mol^{-1}}$ and $\sigma = 4.07\,\text{Å}$, which was obtained by averaging the non-bonded parameters over all atoms in an 8CB molecule. A cut-off radius of 100 Å was employed in the calculations. The potential energy was evaluated over a three-dimensional grid of points, covering one unit mesh of the surface, at a nominal pitch of 0.1 Å, out to a distance of 20 Å from the surface. The potential energies were then averaged along the y-direction (chain axis) to produce a two-dimensional potential energy function. The calculation was performed for the (1 0 0) and (1 1 0) faces of PE.

The averaging of the potential energy in the y-direction is justified by the fact that there is very little variation in potential energy along the chain axis when using a united atom model, despite the planar zig-zag conformation of the PE chain. For example, for the polyethylene (1 0 0) surface, the position of the potential well varies by less than 0.1 Å while the variation in well depth is approximately $0.3\,\mathrm{kJ\,mol^{-1}}$ along the chain axis. The use of a single average pair of energy parameters in the evaluation of the Lennard–Jones potential represented a compromise. Ideally, a separate calculation should have been performed with each pair of atom types present in the model. This would have added greatly to the effort required to implement the PE potential energy function. However, it was felt that the potential energy function was sufficiently crude that the differences produced by introducing different atom types would be negligible compared with the distortions introduced by the fitting procedure (see below). Nevertheless, we envisage using Lorentz–Berthelot mixing rules [36] to improve the quality of the PE pseudopotential in future work.

The complete explicitly calculated and averaged potential energy function is shown in figures 3 (*a*) and 4 (*a*) for the (1 0 0) and (1 1 0) surfaces of PE, respectively.

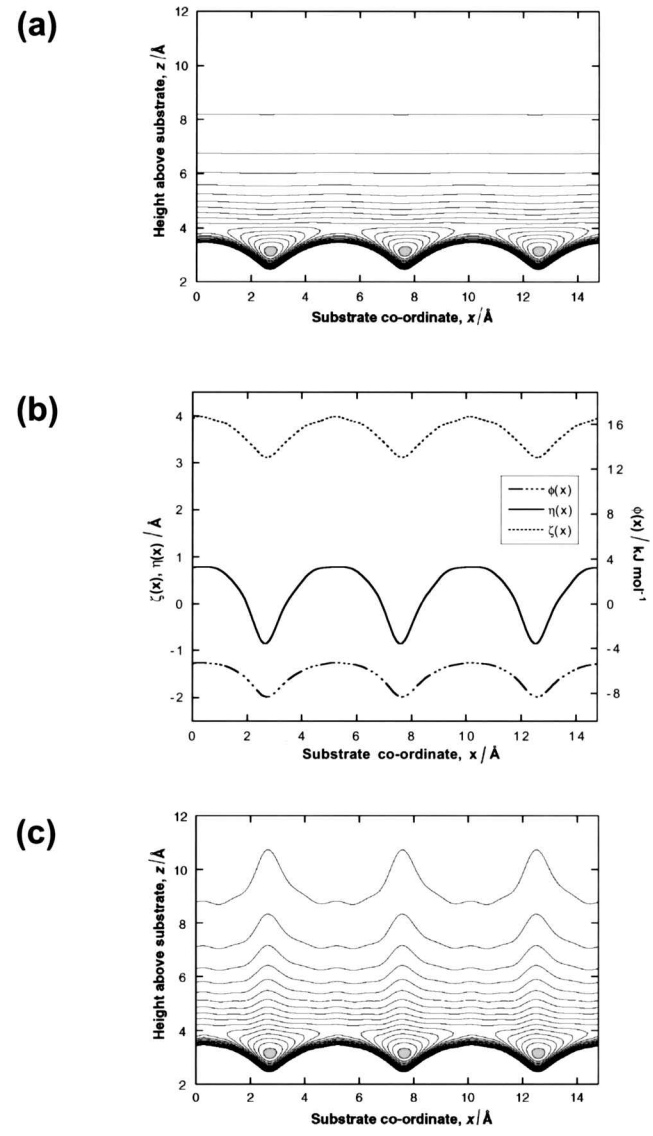

Figure 3. (*a*) The potential energy above the (1 0 0) face of a polyethylene crystal, calculated using pairwise Lennard–Jones potentials, and averaged along the polymer chain axis (y-axis). (*b*) The functions $\phi(x)$, $\eta(x)$ and $\zeta(x)$, determined during the fitting of equation (13) to the data shown in (*a*). (*c*) The final pseudopotential energy function using the Fourier coefficients listed in table 1. In (*a*) and (*c*) the minimum potential energy regions are indicated by shading, the contour interval is $0.5\,\mathrm{kJ\,mol^{-1}}$, and only negative energy contours are shown. The extent of the x-axis corresponds to three unit cell repeats perpendicular to the polymer chains in the crystal surface, i.e. the [0 1 0] direction.

It is a straightforward matter to fit the potential energy function in equation (13) to the explicit atom calculation. The position and depth of the well for each value of x, i.e. $\zeta(x)$ and $\phi(x)$, may be measured directly from the explicit atom data, and are thus fixed. The offset, $\eta(x)$, is

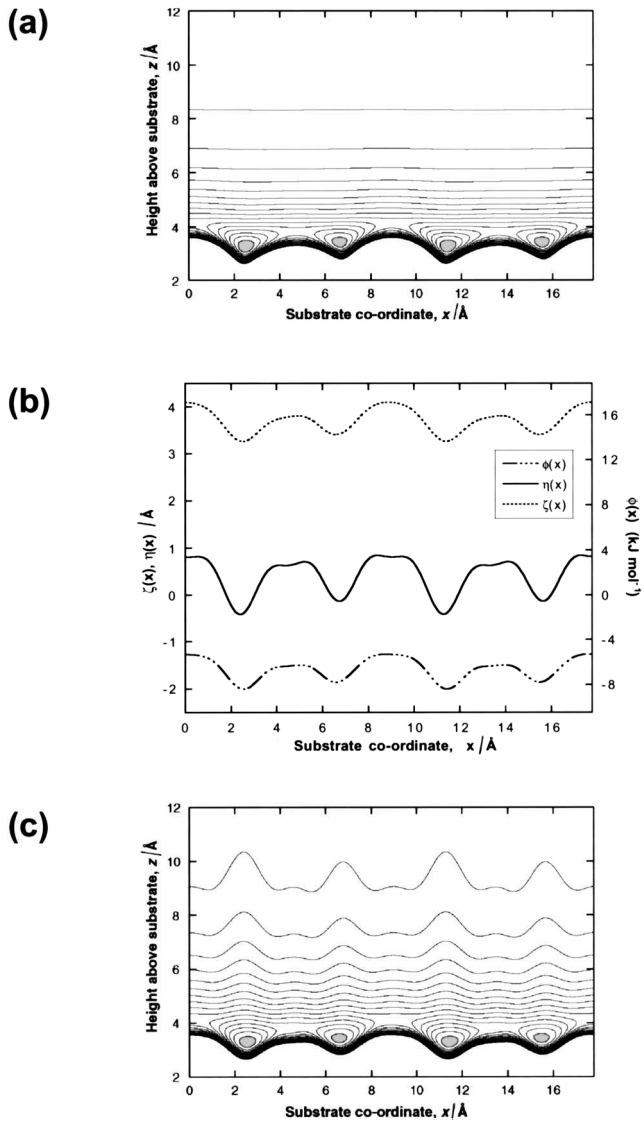

Figure 4. (*a*) The potential energy above the (1 1 0) face of a polyethylene crystal, calculated using pairwise Lennard–Jones potentials, and averaged along the polymer chain axis (*y*-axis). (*b*) The functions $\phi(x)$, $\eta(x)$ and $\zeta(x)$, determined during the fitting of equation (13) to the data shown in (*a*). (*c*) The final pseudopotential energy function using the Fourier coefficients listed in table 2. In (*a*) and (*c*) the minimum potential energy regions are indicated by shading, the contour interval is 0.5 kJ mol^{-1}, and only negative energy contours are shown. The extent of the *x*-axis corresponds to two unit cell repeats, i.e. four polymer chains, in the [1 $\bar{1}$ 0] direction.

then obtained using a least squares procedure, separately, for each value of x. The fitting procedure was restricted to energies less than a limit, U_{max}, in order to ensure that the function was not dominated by the high energy repulsive part of the potential at the expense of the attractive part. A convenient value for U_{max} was found to be 20 kJ mol^{-1}. The functions $\zeta(x)$, $\phi(x)$ and $\eta(x)$ that were determined in this way are shown in figures 3(*b*) and 4(*b*), for the (1 0 0) and (1 1 0) surfaces, respectively.

The final stage in the fitting process is to replace $\zeta(x)$, $\phi(x)$ and $\eta(x)$ with Fourier series:

$$\zeta(x) = \frac{\zeta_0}{2} + \sum_{k=1}^{\infty}\left(\zeta_k \cos\frac{2k\pi x}{\lambda} + \zeta'_k \sin\frac{2k\pi x}{\lambda}\right)$$

$$\phi(x) = \frac{\phi_0}{2} + \sum_{k=1}^{\infty}\left(\phi_k \cos\frac{2k\pi x}{\lambda} + \phi'_k \sin\frac{2k\pi x}{\lambda}\right) \quad (14)$$

$$\eta(x) = \frac{\eta_0}{2} + \sum_{k=1}^{\infty}\left(\eta_k \cos\frac{2k\pi x}{\lambda} + \eta'_k \sin\frac{2k\pi x}{\lambda}\right).$$

The Fourier coefficients in equation (14) are summarized in table 1 for the (1 0 0) surface and table 2 for the (1 1 0) surface. In both cases, five terms were found to be more than sufficient for an accurate representation of $\zeta(x)$, $\phi(x)$ and $\eta(x)$. The final potential energy function represented by equations (13) and (14) is shown in figures 3(*c*) and 4(*c*) for the (1 0 0) and (1 1 0) surfaces respectively.

The contours drawn in figures 3 and 4 represent the attractive parts of the potential energy of the PE crystal surfaces. It can be seen that there is good agreement between the explicit calculation and equation (13), with the shapes of the potential wells being captured accurately. However, there is a region above each of the wells in which the contours bend away from the horizontal in the plots of equation (13), and the fit to the explicit calculation appears poorest. This failure is a consequence of the fact that the assumptions made in integrating the Lennard–Jones potential, i.e. that the surfaces are flat and of uniform atomic density, are least valid in the troughs of the molecular corrugations, with the result that the functional form of equation (13) is not ideal in these regions. The main effect of this deviation will be that any aligning influence exerted by the substrate on the liquid crystal molecules in our simulations will be longer range than expected. However, the effect is likely to be small compared with the influence of any surrounding liquid crystal molecules.

5. Materials and simulation methods

Molecular dynamics simulations were performed using single molecules of the liquid crystal 4-*n*-octyl-4′-cyanobiphenyl (8CB) (see figure 1) in contact with the *E*-modulated and σ-modulated cosine pseudopotentials described above. 8CB was chosen because it is a simple rod-like liquid crystal, whose behaviour has been well characterized in the past [37–40].

In all of the cosine pseudopotential simulations, the value $n = 0.0435$ Å^{-3} was used, which represents the number density of CH_2 groups found in the unit cell of

Table 1. The Fourier coefficients for the (1 0 0) surface of polyethylene. The wavelength of the surface corrugation is 4.930 Å. These coefficients were determined using an origin at the bottom of the molecular corrugation, corresponding to the point $x = 2.7$ Å in figure 3.

k	ζ_k/Å	ζ'_k/Å	ϕ_k/kJ mol^{-1}	ϕ'_k/kJ mol^{-1}	η_k/Å	η'_k/Å
0	7.2857	—	− 12.656	—	5.1024×10^{-1}	—
1	-3.8909×10^{-1}	-1.2159×10^{-2}	− 1.3335	-1.0727×10^{-1}	-7.2357×10^{-1}	3.6063×10^{-3}
2	-8.8383×10^{-2}	2.5899×10^{-3}	-4.0975×10^{-1}	-1.1273×10^{-2}	-2.4044×10^{-1}	2.2573×10^{-2}
3	-3.4811×10^{-2}	-6.8372×10^{-4}	-1.5340×10^{-1}	1.7077×10^{-3}	-8.0614×10^{-2}	2.5912×10^{-2}
4	-3.0442×10^{-3}	3.2170×10^{-4}	-5.8183×10^{-2}	3.5860×10^{-3}	-4.8260×10^{-2}	2.1280×10^{-2}
5	-1.4022×10^{-2}	-6.9747×10^{-4}	-2.6996×10^{-2}	2.1831×10^{-3}	-1.4554×10^{-2}	5.9132×10^{-3}

Table 2. The Fourier coefficients for the (1 1 0) surface of polyethylene. The wavelength of the surface corrugation is 8.892 Å. These coefficients were determined using an origin at the bottom of the first molecular corrugation in figure 4, at the point $x = 2.5$ Å.

k	ζ_k/Å	ζ'_k/Å	ϕ_k/kJ mol^{-1}	ϕ'_k/kJ mol^{-1}	η_k/Å	η'_k/Å
0	7.4022	—	− 13.244	—	7.9470×10^{-1}	—
1	-7.9534×10^{-2}	-1.5873×10^{-1}	-3.0160×10^{-1}	-5.7636×10^{-1}	-1.3018×10^{-1}	-8.4854×10^{-2}
2	-2.8878×10^{-1}	5.3286×10^{-2}	− 1.0695	1.7709×10^{-1}	-4.8548×10^{-1}	9.2301×10^{-2}
3	-1.0833×10^{-2}	-1.9320×10^{-2}	-8.9032×10^{-2}	-1.3427×10^{-1}	-2.4808×10^{-2}	-1.0652×10^{-2}
4	-4.6694×10^{-2}	2.4216×10^{-2}	-2.5745×10^{-1}	1.0677×10^{-1}	-1.5551×10^{-1}	7.4373×10^{-2}
5	-8.4981×10^{-3}	-3.2329×10^{-3}	-4.1806×10^{-2}	-4.1795×10^{-2}	-2.0833×10^{-3}	-7.6183×10^{-3}

polyethylene. The corrugation wavelength of the pseudopotential, λ, took the values 4.0, 5.0 and 6.0 Å, which was considered to be in line with the range of periodicities found in typical polymer crystal surfaces. For the E-modulated potential, we used $\Delta E/E_0 = 0$, 1, 2 and 3, and for the σ-modulated potential, $\Delta\sigma/\sigma_0 = 0.5$, 0.75, 1.0 and 1.25. Again, these values were considered to be consistent with the corrugation amplitudes observed on real polymer crystal surfaces. The $\Delta E/E_0 = 0$ simulation corresponds, of course, to a surface with no corrugation. The values used for E_0 (0.83 kJ mol^{-1}) and σ_0 (4.0677 Å) were taken from the Dreiding 2 force field parameters for interactions between pairs of CH_2 united atoms [35]. The same values of E_0 and σ_0 were used for interactions of the surface with all of the atoms in the liquid crystal molecules.

Further simulations were performed using the polyethylene pseudopotential as the basis of the surface. In this case we made use of the rod-like 8CB molecule, as well as 4-*n*-heptyl-2-fluorophenyl 4-octyloxybiphenyl-4′-carboxylate (MBF), which is known to form a smectic C* phase when suitably doped. Both molecules have been the subjects of previous studies involving atomistic representations of polyethylene surfaces [25–27].

All simulations were performed using the DL_POLY molecular dynamics package [41] which was modified to include the surface potentials described above. The molecular models were constructed using the Cerius2 molecular modelling package [42] which was also used to visualize the molecular dynamics trajectories. The Dreiding 2 force field [35] was used to provide the internal energy terms for the liquid crystal molecules. United atoms were used to replace all CH, CH_2 and CH_3 groups, and the biphenyl torsional potential was modified to avoid planarity as described previously [25]. Van der Waals interactions employed a cut-off radius of 8.5 Å, and electrostatic interactions were not included for reasons mentioned in the introduction. The Dreiding 2 force field was selected, partly because of its simplicity, and partly to allow comparisons to be drawn with earlier work employing the same force field. Since the aim of the project was to study generic features of the behaviour of liquid crystal molecules on polymer substrates, the use of more accurate, and more complex, force fields was felt to be unnecessary.

Molecular dynamics simulations were performed in the microcanonical ensemble at a nominal temperature of 300 K using a 2 fs time step. Each of the simulations consisted of a 10 ps equilibration period, followed by a 200 ns production run. The simulations were carried out on a cluster of 400 MHz Pentium II PCs, running the Linux operating system.

For each of the simulations, orientation distribution functions (ODFs) were calculated separately for the rigid cores and tails of the liquid crystal molecules. The orientation of each molecular fragment was obtained by finding the principal axes of its moment of inertia tensor. The cosine pseudopotential ODFs had mirror symmetry both parallel and perpendicular to the corrugations, and were mapped onto the range 0° to 90°. However, for

the PE pseudopotential simulations, the ODFs are presented for the range $-90°$ to $+90°$, since only a two-fold rotational symmetry was found.

6. Results

As described above, a series of molecular dynamics simulations was performed consisting of a single liquid crystal molecule in contact with a range of pseudopotential surfaces.

6.1. *8CB on E-modulated pseudopotential surfaces*

Figure 5 shows the ODFs obtained for the molecular cores and alkyl tails of an 8CB molecule in contact with a series of *E*-modulated surfaces. It appears that the principal effect of the *E*-modulated potential is to induce alignment of both the cores and tails of the 8CB molecule parallel to the corrugation direction, defined here as 0°. The degree of alignment increases as the potential wells of the corrugations become deeper, and decreases as the corrugation wavelength increases, as can be seen more clearly by examining the peak widths for the distributions (figure 6). It can also be seen that the tails are less well oriented than the cores, with broader peaks in each case. We choose to show peak widths rather than P_2 values in figure 6, because the presence of off-axis features (see below) renders the P_2 values misleading.

As expected, for $\Delta E/E_0 = 0$, there is no preferred orientation. For $\Delta E/E_0 = 1$, the molecule still explores all possible orientations, but has a preference for the substrate chain axis. The tendency to take up orientations away from the chain axis diminishes further for $\Delta E/E_0 = 2$ and 3. In fact, examination of the simulation trajectories shows that, for $\Delta E/E_0 = 2$ and 3, the motion of the 8CB molecule consists of significant periods during which the molecule is aligned parallel to the potential corrugations, punctuated by 180° rotational jumps. This is illustrated by figure 7, which shows the angle of the 8CB core versus time, for simulations with $\lambda = 5.0$ Å and $\Delta E/E_0 = 1$, 2 and 3. The number of 180° jumps observed diminishes as the corrugations become deeper and wider; in fact, for $\lambda = 6.0$ Å and $\Delta E/E_0 = 3$ (not shown here) no jumps were observed during the entire 200 ns simulation.

For the simulations with $\lambda = 4.0$ Å, a second peak is observed in the core ODFs, at an angle of approximately 28° to the chain axis. The exact angle of the peak varies slightly with corrugation depth. There is also a shallow peak centred around 41° in the tail ODFs. The origin of these peaks may be elucidated by a careful examination of the simulation trajectories. In all simulations, the liquid crystal molecules spend the majority of their time with their cores lying parallel to the corrugations, and localized to the region of one of the potential wells, see figure 8 (*a*). In this arrangement, both the rigid core and the flexible tail are able to sample the lowest energy states of the system. Occasionally, however, the molecule rotates so that the core effectively straddles a corrugation, see figure 8 (*b*). In this configuration, groups of atoms at both sides of the biphenyl core fall conveniently over adjacent potential wells, as indicated by the boxes in figure 8 (*b*). In fact, the geometry of the biphenyl core is ideal for this configuration to occur, with the width of the molecules being approximately 4.2 Å when tilted by 30°, see figure 8 (*c*). When the corrugation wavelength is significantly different from 4 Å, such a fortuitous juxtaposition of the biphenyl atoms with the surface corrugations cannot occur, and the off-axial orientation is not favoured. However, this is not a complete explanation, because it fails to account for the off-axial orientation which is found on PE surfaces (see below) in which λ is close to 5 Å. It appears, therefore, that the shapes of the corrugations must be important, as well as their period. The broad off-axial peak in the tail ODFs may also be explained in terms of different parts of the alkyl tail lying in adjacent potential wells.

6.2. *8CB on σ-modulated pseudopotential surfaces*

The behaviour of the 8CB molecules in contact with the σ-modulated pseudopotential is superficially the same as that with the *E*-modulated pseudopotential. The ODFs for the cores and tails of the molecules in contact with a range of surfaces are shown in figure 9. As previously, there is a marked tendency for the cores to align parallel to the corrugations. However, the alignment is less pronounced than in the *E*-modulated case, the distributions being both broader and flatter. The peak widths for the cores are shown in figure 10. In general, the alignment improves both as the corrugation wavelength decreases and as the corrugation depth increases, just as for the *E*-modulated case. However, there are some discrepancies that will be discussed below. In addition, for $\lambda = 4.0$ Å, there is evidence of a slight tendency to align perpendicular to the corrugations. The behaviour of the tails is somewhat different, in that there is only a slight preference for them to align with the corrugations. The peak widths for the tails are not shown in figure 10 because they are too indistinct to measure accurately.

An explanation for the broadness of the peaks in the σ-modulated ODFs compared with the *E*-modulated cases may be found by examining the trajectory of the 8CB molecule during the simulation. As with the *E*-modulated simulations, the trajectories consist of periods in which the molecule explores configurations roughly parallel to the corrugations, punctuated with 180° rotational jumps about an axis perpendicular to the surface. However, the intervals between jumps are less well defined than in the *E*-modulated case. Figure 11 shows 10 consecutive configurations of the 8CB molecule taken at 2 ps intervals

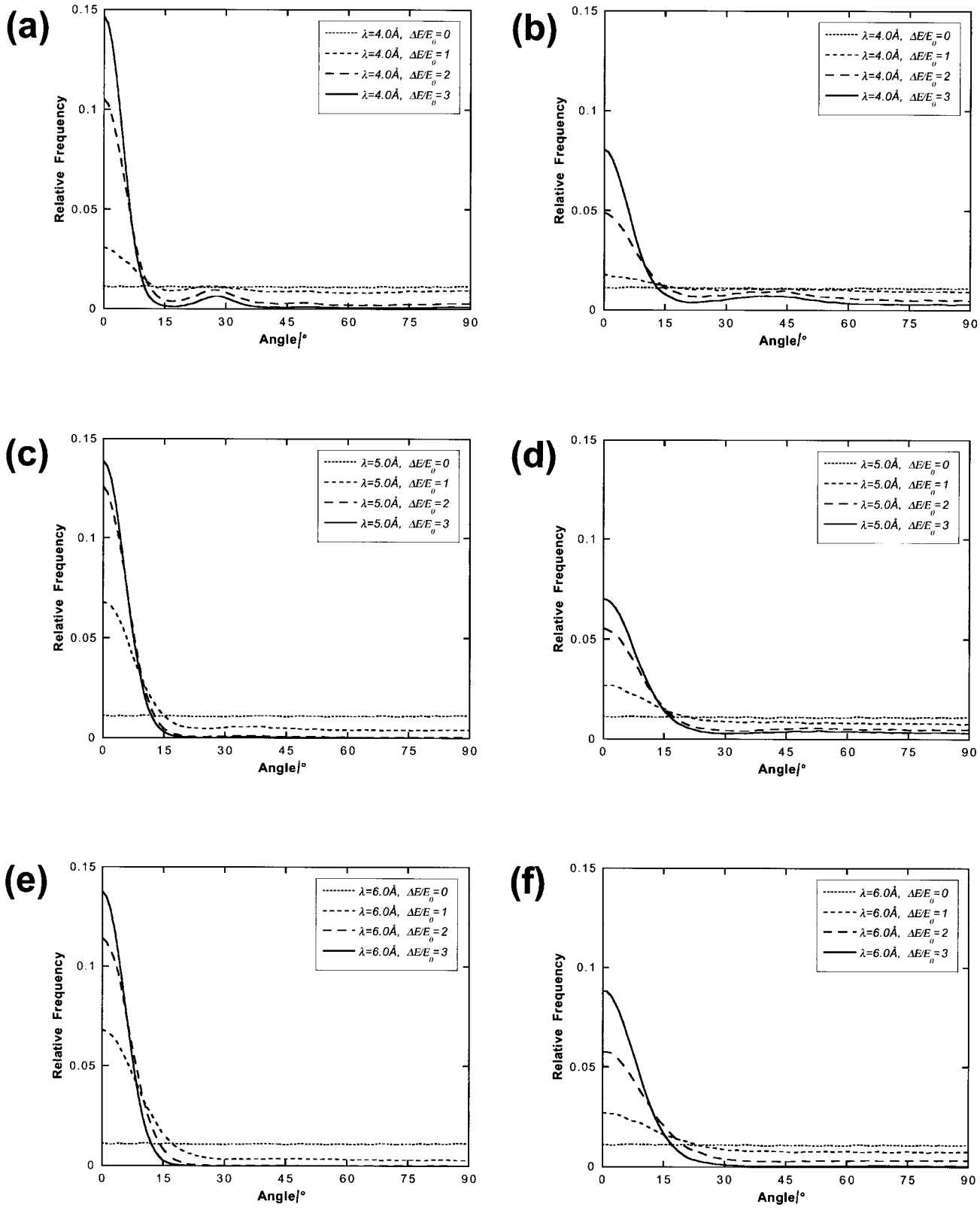

Figure 5. ODFs for the cores and tails of isolated 8CB molecules in contact with a wall represented by the *E*-modulated pseudopotential of equation (6), with $\Delta E/E_0 = 0$, 1, 2 and 3, and corrugation wavelengths of 4.0, 5.0 and 6.0 Å. In these ODFs, 0° corresponds to a direction parallel to the corrugations, i.e. the substrate chain axis, and 90° is perpendicular to them. (*a*) $\lambda = 4.0$ Å, cores; (*b*) $\lambda = 4.0$ Å, tails; (*c*) $\lambda = 5.0$ Å, cores; (*d*) $\lambda = 5.0$ Å, tails; (*e*) $\lambda = 6.0$ Å, cores; (*f*) $\lambda = 6.0$ Å, tails.

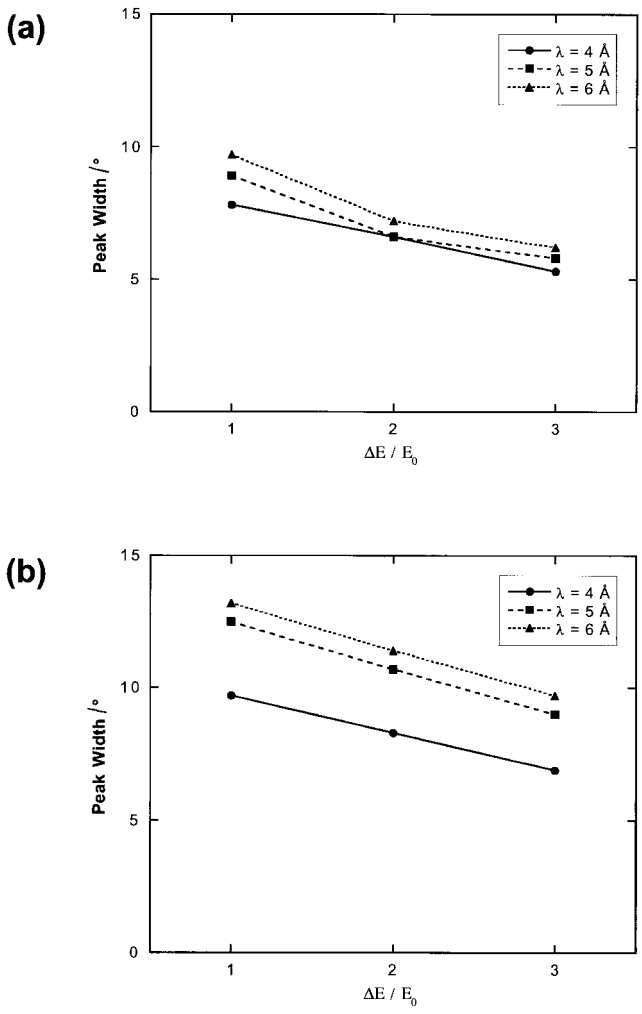

Figure 6. Graph showing values of the half-width at half-height of the main ODF peaks for (*a*) the molecular cores and (*b*) the alkyl tails of an 8CB molecule in contact with various *E*-modulated pseudopotential surfaces.

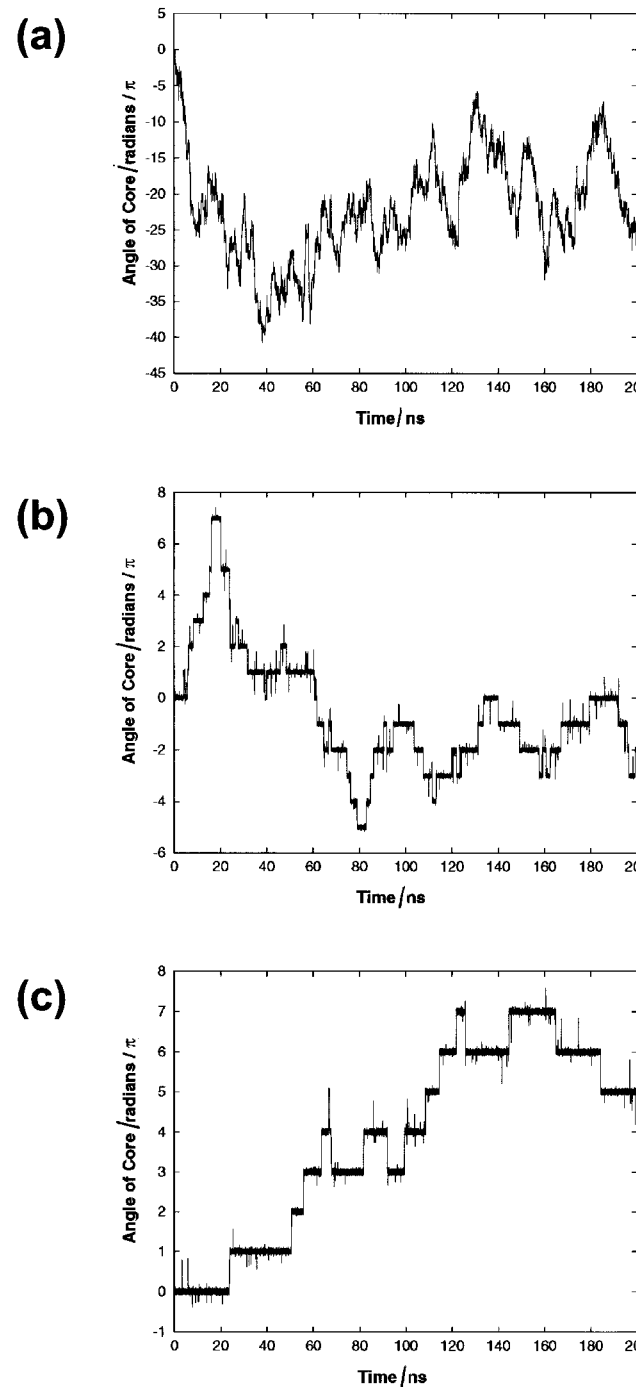

Figure 7. The angle of the 8CB core versus time, for simulations with $\lambda = 5.0$ Å. (*a*) $\Delta E/E_0 = 1$; (*b*) $\Delta E/E_0 = 2$; (**c**) $\Delta E/E_0 = 3$. The punctuated nature of the motion is clear for the deeper corrugations. The angles have been 'unwrapped' so that each full rotation increases the angle by 2π.

from a simulation with $\lambda = 4.0$ Å and $\Delta\sigma/\sigma_0 = 1.0$. In figure 11 (*a*), the molecules are seen from above, and it is clear that they tend to sit *above* the peaks of the corrugations, rather than between them, which had been the expectation when the potential was originally developed. In figure 11 (*b*), the molecules are viewed end-on, and superimposed on a contour plot of the potential energy profile. It is clear from this view that some parts of the molecules penetrate the troughs of the corrugations, contributing to the breadth of the ODF peaks, but in general it is found that the centres of mass of the molecules favour the tops of the corrugations.

6.3. *8CB on (1 0 0) and (1 1 0) PE surfaces*

The simulations of 8CB molecules on parameterized PE surfaces yielded rather different results from those observed using cosine pseudopotentials. The ODFs are shown in figure 12 for both the (1 0 0) and (1 1 0) surfaces. Rather than a single peak at 0°, the core ODFs in both cases display several large peaks corresponding to preferred orientations that are not parallel to the corrugations. The ODFs appear qualitatively similar,

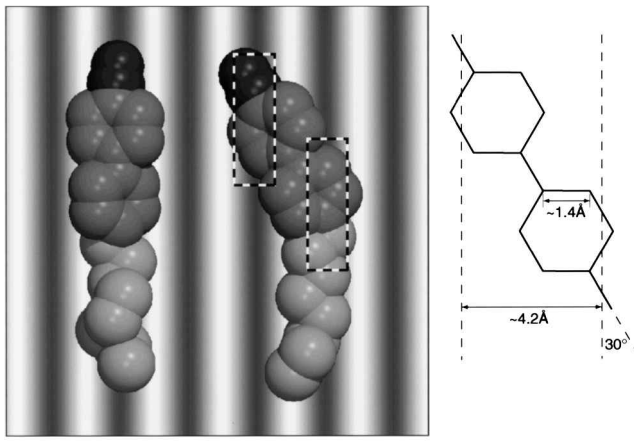

Figure 8. (*a*) and (*b*): Two conformations of the 8CB molecule, taken from an *E*-modulated pseudopotential simulation with $\lambda = 4.0$ Å and $\Delta E/E_0 = 3$, superimposed upon a periodic greyscale which represents the pseudopotential The alkyl tail is shown in light grey, the biphenyl is medium grey, and the cyano group is dark grey; the dark fringes represent the positions of the lowest energy potential wells, shown shaded in figure 2 (*a*). The *x*-axis is horizontal and the *y*-axis vertical. In (*b*), the core atoms that occupy low energy positions are indicated with boxes. (*c*) Schematic diagram showing how a tilt of 30° results in groups of atoms on both sides of the biphenyl core lining up with corrugations approximately 4 Å apart.

with minor variations in the positions of the peaks that are probably a consequence of the different spacing between substrate corrugations in the two cases, i.e. 4.93 Å for the (1 0 0) surface and 4.45 Å for the (1 1 0) surface.

On the (1 0 0) surface, the main ODF peaks are at − 11° and + 27°, while on the (1 1 0) surface they are at − 15° and + 30°. The reason for the asymmetry appears to be mainly that the 8CB molecule does not rotate about its long axis for the entire duration of each simulation (200 ns). Such rotations were common in the cosine pseudopotential simulations, because the cosine potentials were less attractive than the PE ones. The PE pseudopotentials themselves possess a near reflection symmetry about the bottoms of the potential wells, and so are unlikely to be having a major effect on the symmetry of the ODFs. The positions of the peaks are summarized in table 3, together with the results from previous simulations that used atomistic substrates [26]. Within measurement errors, the positions of the peaks agree well between the two methods, but the longer simulation time and better sampling statistics in the present case makes it possible to identify additional peaks.

The origins of each of the peaks in the core ODFs may be identified by examining the molecular dynamics

Table 3. The peak positions for the core ODFs taken from simulations of single 8CB molecules in contact with various polyethylene surfaces. The atomistic data were taken from [26] and mapped onto the range − 90° to + 90°. The uncertainties in the pseudopotential peak positions are ± 1° except where stated otherwise; those of the atomistic peak positions are ± 5°.

Surface	Representation	Peak positions/°
(1 0 0)	Pseudopotential	− 34, − 11, + 3, + 27
	Atomistic [26]	− 10, + 30
(1 1 0)	Pseudopotential	− 38 ± 2, − 15, + 3, + 30
	Atomistic [26]	− 19, + 25

trajectory. Figure 13 shows eight configurations taken from the simulation of 8CB on the (1 0 0) PE surface. The configurations shown were extracted from a 1 ns interval, but are typical of those observed throughout the 200 ns simulation. The dark bands in the background represent the low energy corrugation troughs between the polymer chains in the substrate. Those atoms of the core that lie above the low energy troughs are indicated by boxes. For each of the most common configurations, one or two groups of core atoms coincide with a corrugation trough.

The most common off-axial alignments are shown in figures 13 (*a*) and 13 (*b*), which correspond to the ODF peak at + 27°, and figures 13 (*e*) and 13 (*f*), which correspond to the ODF peak at − 11°. In figure 13 (*a*), the 8CB molecule straddles one of the substrate polymer chains, with parts of the biphenyl core lying in two adjacent troughs. This behaviour is reminiscent of that shown for the cosine pseudopotential in figure 8 (*b*). However, the configuration shown in figure 13 (*b*) appears equally common. In this configuration, the molecule is translated by half of a corrugation period to one side, so that half of the biphenyl atoms occupy low energy positions. In the configurations shown in figures 13 (*e*) and 13 (*f*), on the other hand, low energy is achieved when the atoms on one side of one benzene ring lie over a corrugation trough. In addition, in figure 13 (*e*) the cyano group assumes a favourable position energetically, while in figure 13 (*f*) the first atom of the alkyl tail also contributes to the lowering of the energy. In both cases, the rest of the molecular core lies across the peak of the substrate corrugation.

The configurations shown in figures 13 (*g*) and 13 (*h*) correspond to the ODF peak at − 34°. They are analogous to those shown in figures 13 (*b*) and 13 (*a*), respectively, but with the molecule rotated anticlockwise rather than clockwise. While it is possible to obtain orientations with the liquid crystal core approximately parallel to the corrugations, e.g. figure 13 (*c*) and 13 (*d*), this type of configuration results in most of the core

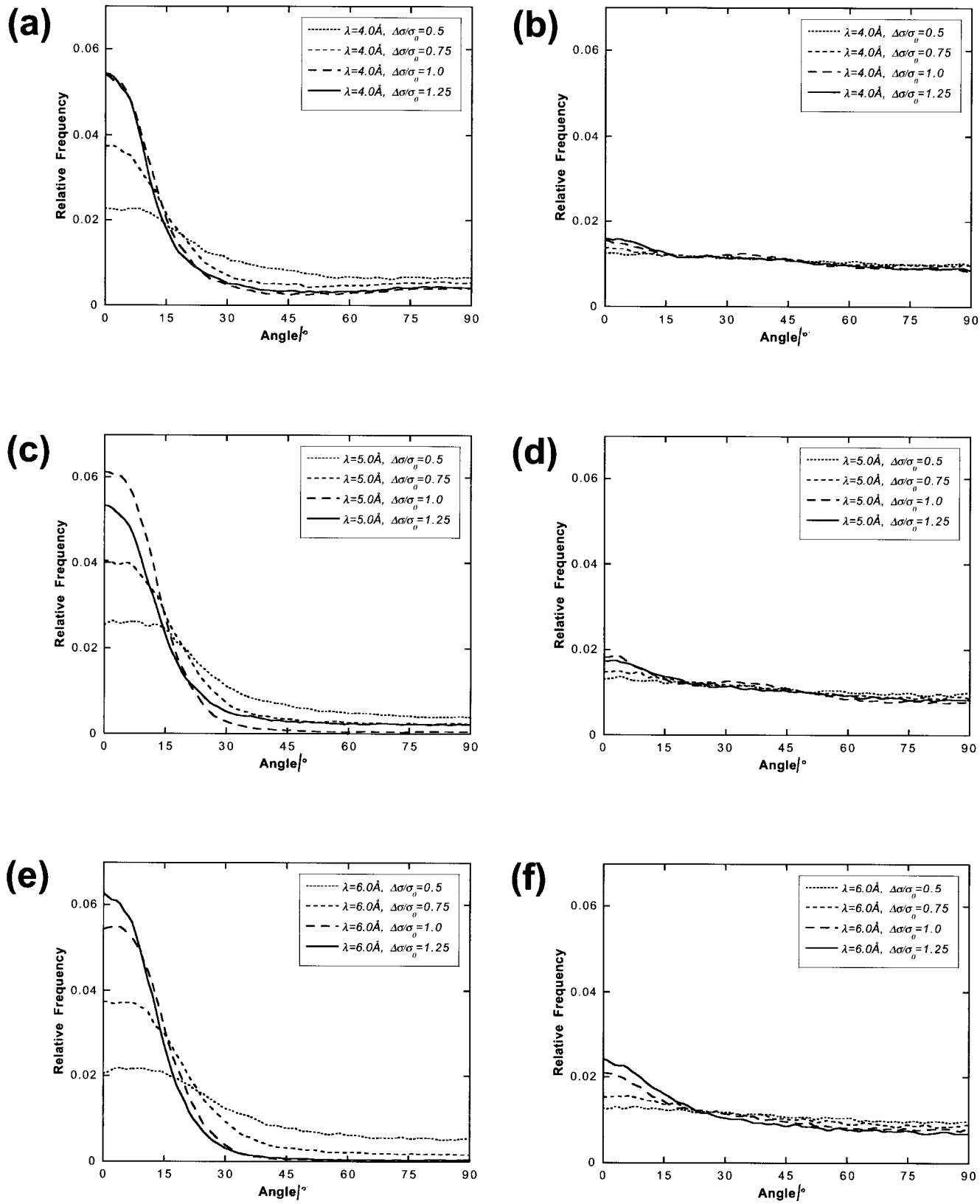

Figure 9. ODFs for the cores and tails of isolated 8CB molecules in contact with a wall represented by the σ-modulated pseudopotential of equation (9), with $\Delta\sigma/\sigma_0 = 0.5$, 0.75, 1.0 and 1.25, and corrugation wavelengths of 4.0, 5.0 and 6.0 Å. (*a*) $\lambda = 4.0$ Å, cores; (*b*) $\lambda = 4.0$ Å, tails; (*c*) $\lambda = 5.0$ Å, cores; (*d*) $\lambda = 5.0$ Å, tails; (*e*) $\lambda = 6.0$ Å, cores; (*f*) $\lambda = 6.0$ Å, tails.

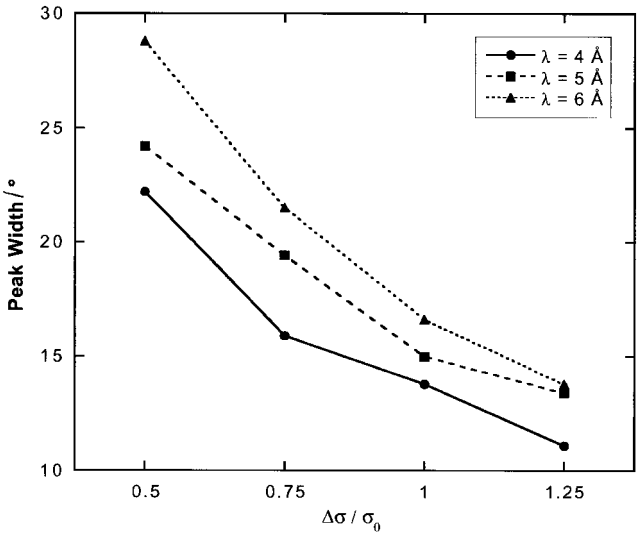

Figure 10. Graph showing values of the half-width at half-height of the main ODF peaks for the cores of an 8CB molecule in contact with various σ-modulated pseudopotential surfaces.

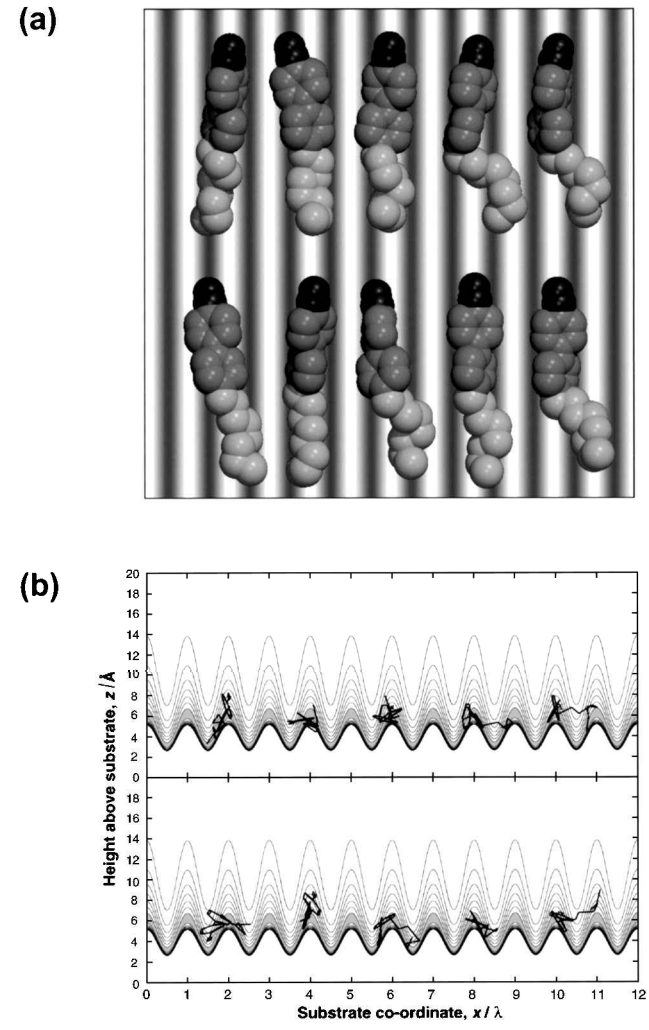

Figure 11. Ten conformations, taken at 2 ps intervals, from a simulation using a σ-modulated pseudopotential with $\lambda = 4.0$ Å and $\Delta\sigma/\sigma_0 = 1.0$. In (*a*), the molecules are viewed from above and the pseudopotential is represented by a periodic greyscale. The topographic peaks of the corrugations, shown in figure 2 (*b*), are represented by white, and the troughs by dark grey. In (*b*), the same molecules are shown in stick representation, looking along the axis of the corrugations. In this case, the molecules are superimposed on the potential energy contours of the pseudopotential. The contour interval is 0.5 kJ mol^{-1} and only negative energy contours are shown. The position of the potential well is indicated by shading.

atoms occupying high energy positions, and so it is not particularly common. The above analysis is very simplistic but accounts for the gross behaviour of the molecules; the actual orientations assumed by the 8CB molecule are dependent on many competing energetic factors. However, a similar pattern of behaviour is observed on the (1 1 0) surface with minor variations due to the slight differences in corrugation depth and width compared with the (1 0 0) surface.

The ODFs for the tails show less pronounced orientations than for the cores. Indeed, in the (1 0 0) case there is little evidence for any preference in orientation. P_2 values were computed from the tail ODFs using $P_2 = \langle 1/2(3\cos^2\theta - 1)\rangle$, where θ is the angle between the major axis of the molecular fragment and the corrugation direction. The P_2 value obtained for the tails in this case is 0.31, which is not much greater than the value of 0.25 expected for an unoriented two-dimensional system. On the (1 1 0) surface, the main preference is for orientation parallel to the surface corrugations, with additional preferences at $\pm 30°$. In this case the P_2 value is still low, at 0.39. These results are somewhat different from those obtained using atomistic substrates [26]. In our previous work, there was a much stronger preference for the alkyl tails to lie parallel to the molecular corrugations of the PE surface, in what resembled an epitaxial arrangement. The P_2 values were correspondingly higher, at 0.49 for the (1 0 0) surface and 0.55 for the (1 1 0) surface.

6.4. *MBF on (1 0 0) and (1 1 0) PE surfaces*

The ODFs for single MBF molecules on the (1 0 0) and (1 1 0) surfaces of PE are shown in figure 14. In both cases, the cores show several preferred orientations that are not parallel to the polymer chain axis. As was the case for 8CB, the asymmetry in the ODFs is ascribed to the fact that the liquid crystal molecule does not rotate about its long axis for the duration of the 200 ns simulation. The behaviours of the cores on the two surfaces appear to be quite similar, with the biggest difference being that, on the (1 0 0) surface there is a large peak at $-16°$ with a shoulder at $-24°$, while on

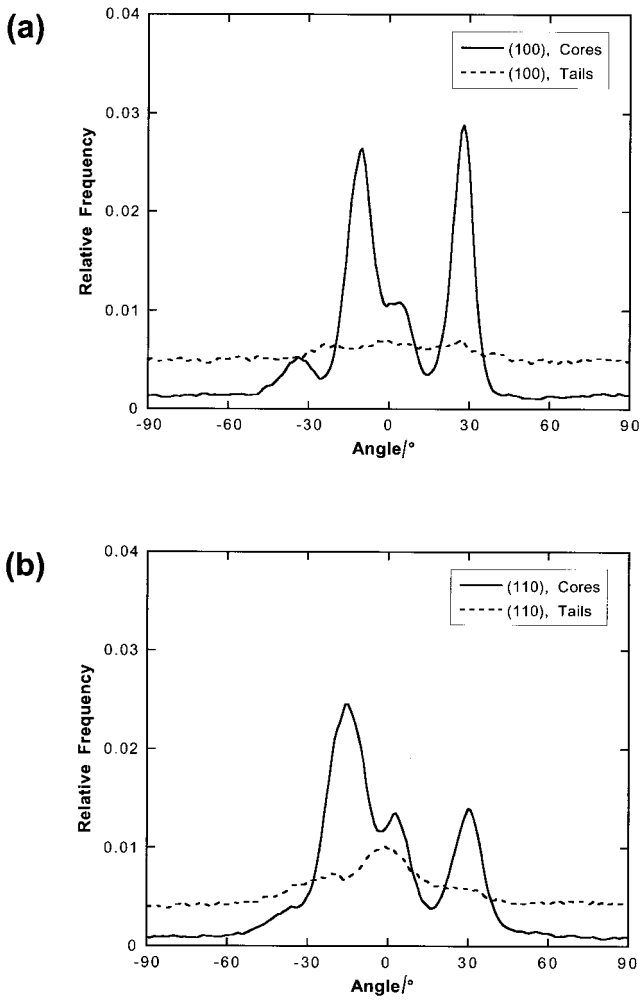

Figure 12. ODFs for the cores and tails of a single molecule of 8CB on (*a*) the (1 0 0) and (*b*) the (1 1 0) surfaces of crystalline polyethylene. The polyethylene surface is represented by equation (13).

the (1 1 0) surface there are two equal sized peaks at − 19° and − 29°. The differences in angle between the peaks for the two surfaces appear to result from the small difference in periodicity of the two surfaces.

Table 4 summarizes the MBF core orientations for both surfaces, and compares them with the results from simulations using atomistic surfaces that were presented in [27]. It can be seen that, while the two methods produce many peaks at approximately the same angles, there are distinct differences. For example, on the (1 0 0) surface, the pseudopotential simulations produced peaks at − 42° and + 27° that were not observed in the atomistic simulations, while the atomistic simulations displayed a broad peak at + 60° that was not seen in the pseudopotential case. The most obvious discrepancy on the (1 1 0) surface is that the strong peak at − 29° in the pseudopotential ODF is missing from the atomistic ODF. The most likely explanation for these differences

Table 4. The peak positions for the core ODFs taken from simulations of single MBF molecules in contact with various polyethylene surfaces. The atomistic data were taken from [27] and mapped onto the range − 90° to + 90°. The uncertainties in the pseudopotential peak positions are ± 1°; those of the atomistic peak positions are ± 3° except where stated otherwise.

Surface	Representation	Peak positions/°
(1 0 0)	Pseudopotential	− 42, − 24, − 16, + 5, + 27, + 43
	Atomistic [27]	− 25, − 11, + 13, + 42, + 60 ± 10
(1 1 0)	Pseudopotential	− 29, − 19, + 5, + 33
	Atomistic [27]	− 75, − 21, + 6, + 37

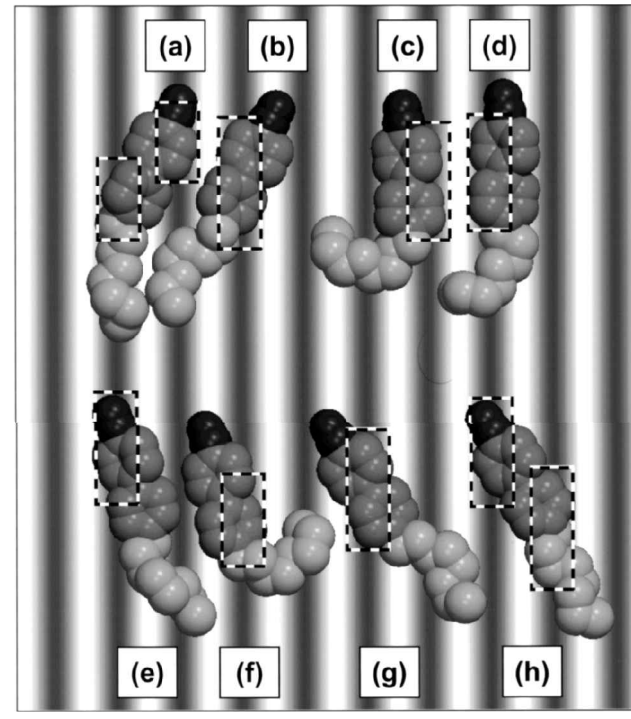

Figure 13. Eight configurations taken from the single molecule simulation of 8CB on the (1 0 0) surface of polyethylene, illustrating how each of the peaks in the core ODF arises. The dark bands in the background represent the low energy troughs between the polyethylene chains in the substrate. In each case, the core atoms in lowest energy positions are indicated by boxes. The approximate angles of the cores in each case are: (*a*) + 25°; (*b*) + 26°; (*c*) − 2°; (*d*) 0°; (*e*) − 16°; (*f*) − 13°; (*g*) − 31°; (*h*) − 30°.

is that the duration of the atomistic simulations was only 4 ns compared with 200 ns for the pseudopotential simulations, so that the relative heights of the atomistic ODF peaks are considerably less reliable than those of the pseudopotential peaks. There may also be minor differences in peak position caused by the pseudopotential itself, resulting from the fact that it is not a perfect representation of the atomistic potential. This

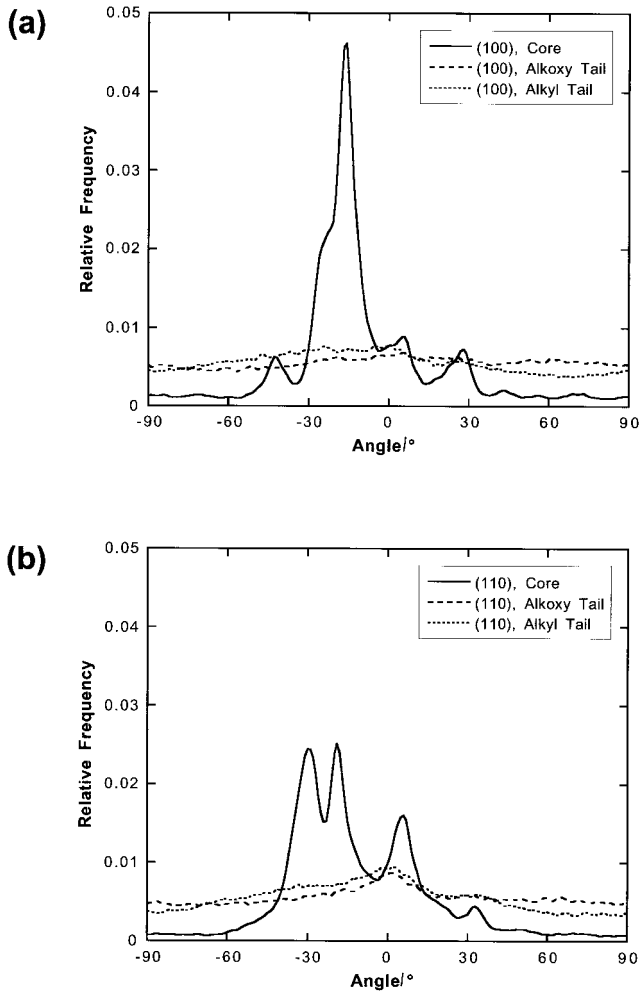

Figure 14. ODFs for the cores and tails of a single molecule of MBF on (*a*) the (1 0 0) and (*b*) the (1 1 0) surfaces of crystalline polyethylene. The polyethylene surface is represented by equation (13).

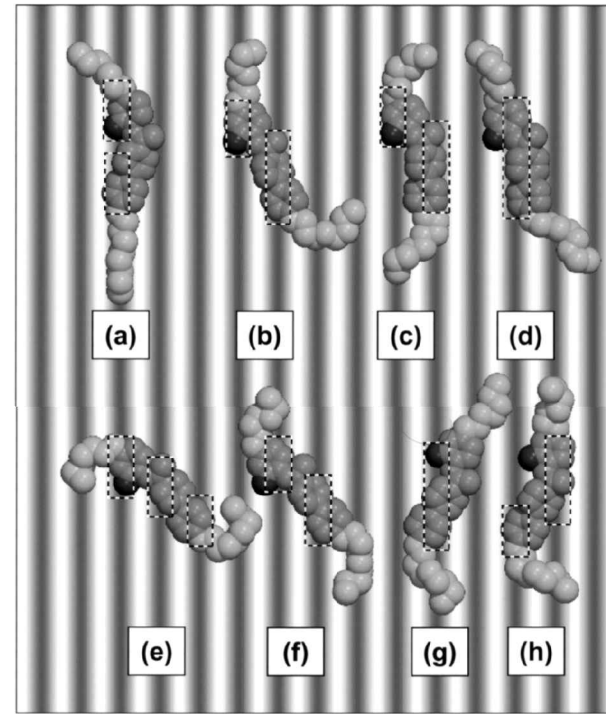

Figure 15. Eight configurations taken from the simulation of a single molecule of MBF on the (1 0 0) surface of polyethylene, illustrating how each of the peaks in the core ODF arises. The dark bands in the background represent the low energy troughs between the polyethylene chains in the substrate. In each case, the core atoms in lowest energy positions are indicated by boxes. The approximate angles of the cores in each case are: (*a*) + 7°; (*b*) − 23°; (*c*) − 14°; (*d*) − 15°; (*e*) − 43°; (*f*) − 40°; (*g*) + 30°; (*h*) + 28°.

will be discussed further below. Overall, however, the agreement appears to be acceptable.

The origins of the peaks in the core ODFs may be identified by examining the trajectory of the MBF molecule. This is illustrated in figure 15 which shows eight typical configurations of the MBF molecule, chosen to represent the largest peaks in the ODF for the (1 0 0) surface. The configurations were all taken from a 1 ns interval, but are representative of the behaviour of the molecule throughout the simulation. In each case, the core atoms that coincide with troughs in the surface corrugations are indicated. The general principle that appears to operate is that for each configuration one side of each benzene ring in the core coincides with a trough. Since the core contains three benzene rings, this leads to a large number of possible orientations, many of which straddle one or more substrate corrugations, as was reported previously [27].

However, the assignment of each ODF peak to a particular configuration is not as clear cut as was previously suggested. For example, the peak at − 16° contains configurations that lie in just one trough, e.g. figure 15 (*d*), and configurations which straddle a corrugation and lie in two troughs, e.g. figure 15 (*c*). The same is true of the peak at + 27°, see figures 15 (*g*) and 15 (*h*). In a similar fashion the peak at − 42° contains configurations that straddle either one or two corrugations, with parts of the core lying in either two or three troughs, respectively, see figures 15 (*e*) and 15 (*f*). The conformations of the molecular cores are essentially the same in each of the pairs of configurations described. The main difference between the configurations in each case is a translation of half a corrugation wavelength to either side. A similar set of configurations is found on the (1 1 0) surface.

The ODFs for the liquid crystal tails are similar to those for the 8CB tails. On the (1 0 0) surface there is very little orientational preference for either the alkyl or the alkoxy tail. On the (1 1 0) surface there is a clearer

preference for aligning parallel to the polymer chain axis, with slight evidence for off-axial orientations at $\pm 30°$, as was the case for 8CB. In all cases the degree of alignment was considerably less than was observed in the atomistic simulations.

7. Discussion

7.1. *Cosine pseudopotentials*

The results shown above demonstrate the effectiveness of the pseudopotential approach in establishing how liquid crystal alignment is sensitive to the period and depth of molecular scale corrugations. The results also confirm previous suggestions that the alignment of liquid crystal molecules may be induced by the presence of a surface which is corrugated on the scale of a molecular width. The general finding, from both the *E*-modulated and the σ-modulated pseudopotential simulations, is that the degree of orientation increases both as the depth of the corrugation increases, and as the corrugation wavelength decreases.

The *E*-modulated pseudopotential is more successful at inducing alignment than the σ-modulated pseudopotential. In fact, because the liquid crystal molecule sits above the peaks in the σ-modulated surface, we may suggest that variation in topography plays less of a role in orienting the molecule than variation in potential energy. However, it can be seen that the latter is much smaller for the σ-modulated potential than for the *E*-modulated one. This is illustrated as follows. If an atom traverses the *E*-modulated potential at a height of $\sigma_0/5^{1/6}$ above the origin, i.e. at the height of the potential wells, the difference in energy between the peaks and troughs varies from 3.8 kJ mol^{-1} for $\Delta E/E_0 = 1$ to 11.4 kJ mol^{-1} for $\Delta E/E_0 = 3$. A similar traversal above the corrugations of the σ-modulated potential, at a height of $[\sigma_0 + \Delta\sigma]/5^{1/6}$, gives a variation in energy between 2.2 kJ mol^{-1} for $\Delta\sigma/\sigma_0 = 0.5$ and 3.3 kJ mol^{-1} for $\Delta\sigma/\sigma_0 = 1.25$. It appears, therefore, that the σ-modulated potentials used in this study are effectively shallower than the *E*-modulated ones, and that this explains why the orientation is poorer in the σ-modulated simulations. In fact, in the cases considered there appears to be a monotonic relationship between the effective potential energy variation, as given above, and the degree of orientation indicated by the peak widths in figures 6 and 10. It is also clear that there is an entropic advantage associated with the liquid crystal molecule residing at the top of the corrugation rather than lying in a groove, since the latter would inhibit both molecular rotation and conformational changes. In the *E*-modulated simulations, the difference in potential energy between the top and bottom of the corrugations is sufficient to offset this entropic advantage; in the σ-modulated cases, it is not.

The relative shallowness of the effective potential in the σ-modulated simulations also helps to explain the sensitivity of these simulations to the temperature of the system. For, although a nominal temperature of 300 K was chosen in each case, the actual temperature could vary from this by several degrees. One consequence of this is that the core ODF calculated from the simulation with $\lambda = 6.0$ Å and $\Delta\sigma/\sigma_0 = 1.0$ has a more pronounced and higher peak than that for $\Delta\sigma/\sigma_0 = 1.25$, the latter being run at a higher temperature. The results from the *E*-modulated pseudopotential simulations were found not to be sensitive to temperature in this way.

The factor of $[\sigma_0/\sigma(x)]^3$ was introduced into the σ-modulated functional form to ensure that the minimum potential energy was the same at all points across the corrugations. If the factor is omitted, the potential energy is considerably lower at the top of the corrugation than at the bottom. We have performed simulations using a σ-modulated function similar to equation (9) but without this correction [43]. The results from these simulations suggest that a more clearly defined orientation is achieved as the well depth at the top of the corrugation increases, which serves to emphasise that the degree of alignment is determined principally by the variation in energy, rather than by the topography of the corrugations.

7.2. *PE pseudopotentials*

The results shown in § 6.3 confirm that the PE pseudopotential is capable of reproducing the behaviour of liquid crystalline cores on atomistic substrates extremely reliably, but with a fraction of the computational cost. Where discrepancies are found, the deviations appear to be due to insufficient sampling in the atomistic cases, which leads to variations in the ODF peak heights; in extreme cases, peaks may be completely missed. Minor deviations in peak position may result from small differences in the shapes of the PE pseudopotentials, which in turn result from the various averaging processes that were applied in their derivations.

Another possible reason for the lack of agreement is that we are not comparing exactly the same surfaces in the pseudopotential and atomistic simulations. The atomistic simulations employed a single layer of polymer molecules to represent the surface with the non-bonded interactions truncated at 8.5 Å. This model was used for computational efficiency. On the other hand, the pseudopotential derivation employed a thick crystal slab with a cut-off radius of 100 Å. This results in an approximately uniform energy difference of ~ 1 kJ mol^{-1} between the energies calculated from the two models. However, the effect of the choice of model on the computed forces is small, and unlikely to have a major effect on the results of the simulations.

The PE pseudopotentials successfully reproduced the off-axial alignment previously found in atomistic simulations of both 8CB and MBF cores. However, there was a distinct difference in behaviour between the flexible tails in the pseudopotential and atomistic cases. In the atomistic simulations, the flexible tails showed a pronounced preference to lie parallel to the substrate polymer chain axis. However, in the pseudopotential simulations this was not the case, with the tendency to lie parallel to the corrugations being very slight. In addition, on the (1 1 0) surfaces there was an indication of a preference for the tails to lie at $\pm 30°$ to the corrugation direction.

Examination of the molecular trajectory suggests that, despite the poor orientation seen in the ODFs, some parts of the flexible tails do nevertheless lie in the corrugations. In fact, the $\pm 30°$ orientations appear to correspond to configurations in which different parts of the tail lie in adjacent corrugations. In these cases use of the moment of inertia tensor to define the orientation of the whole tail may be misleading, and it might be more informative to examine the orientations of each segment of the alkyl tail in turn. This shortcoming is not, however, an explanation for the lack of agreement with the atomistic simulations, since the same technique was applied in both cases.

It appears that the reason for the poor agreement between pseudopotential and atomistic simulations in the case of the liquid crystal tails is actually because the potential energy was averaged along the chain axis (y-axis) in the derivation of the pseudopotential, and because this limits the possibilities for epitaxial alignment of the alkyl tails with the PE crystal surface. Despite the fact that the variation in potential well depth and position along the PE chain axis is slight, it would appear to be sufficient to influence the behaviour of the alkyl tails. It appears that the alkyl tails are unable to achieve as low an energy in contact with the smoothed pseudopotential surface as on the atomistic surface, with the result that they become more mobile and less well ordered. By the same token, one might expect a model that contained explicit hydrogen atoms would lead to an enhanced epitaxial arrangement. While it is conceivable that this problem could be overcome by replacing the one-dimensional fit to $\phi(x)$, $\zeta(x)$ and $\eta(x)$ with a two-dimensional fit, including variations along the y-axis, this would add to the computational demands of the pseudopotential method, and careful consideration would be needed to determine whether the approach has any advantages over the direct evaluation of atomistic pair-potentials. There may, indeed, be a case for a hybrid approach, in which the potential energy function is supplemented by an artificial modulation parallel to the y-axis.

A further reason for the tail atoms to be more mobile than expected is that a single energy function was used for all atom types. This simplification reduced the effort required both to derive the parameters for equation (13) (tables 1 and 2), and to implement the potential within DL_POLY. The net effect is that the CH_2 united atoms in the alkyl tails experience a slightly weaker interaction with the pseudopotential than with an atomistic substrate, whereas the atoms in the liquid crystalline core experience a slightly stronger interaction. There might be concern that the mobility of the alkyl tails could affect the core orientations observed. However, this possibility was investigated in our previous publications [26, 27] and it was found that the presence or otherwise of the tails has only a minor effect on the orientational preferences of the liquid crystal core.

7.3. *General comments*

The pseudopotential approach has proved to be a very useful method for gaining insights into the orienting behaviour of liquid crystal molecules on crystalline polymer surfaces. The generic surfaces, represented by the cosine pseudopotential, have demonstrated the dependence of the degree of orientation on corrugation wavelength and depth. They have also highlighted the fact that it is the variations in potential well depth, rather than topography *per se*, which lead to the orienting effect, at least for corrugations with a wavelength of around a molecular width. It is interesting to contrast our findings with those of Berreman [44] who showed that geometric factors alone were sufficient to induce alignment of liquid crystals when the grooves had dimensions much greater than the width of a molecule. However, Berreman also noted that molecular scale interactions, such as are represented in our simulations, were sufficient to override the geometric effects.

There were obvious differences between the orienting effects of the generic surfaces and the PE pseudopotential surfaces. For the most part, the cosine pseudopotential surfaces resulted in an axial alignment of both the rigid liquid crystalline cores and the flexible tails. On the other hand, the PE pseudopotential simulations generated off-axial alignments of the liquid crystal cores, and very poor axial alignment of the flexible tails. This is an intriguing result, because it means that the cosine pseudopotential with $\lambda = 5$ Å and the PE pseudopotential with $\lambda = 4.93$ Å produced very different results. This shows that the wavelength of the corrugation is not sufficient on its own to predict the behaviour of a particular liquid crystal. It is clear that the orienting behaviour results from a subtle interaction between the geometry of the liquid crystal molecule and the *shapes* of the surface corrugations, and in addition that the E-modulated and the σ-modulated pseudopotentials

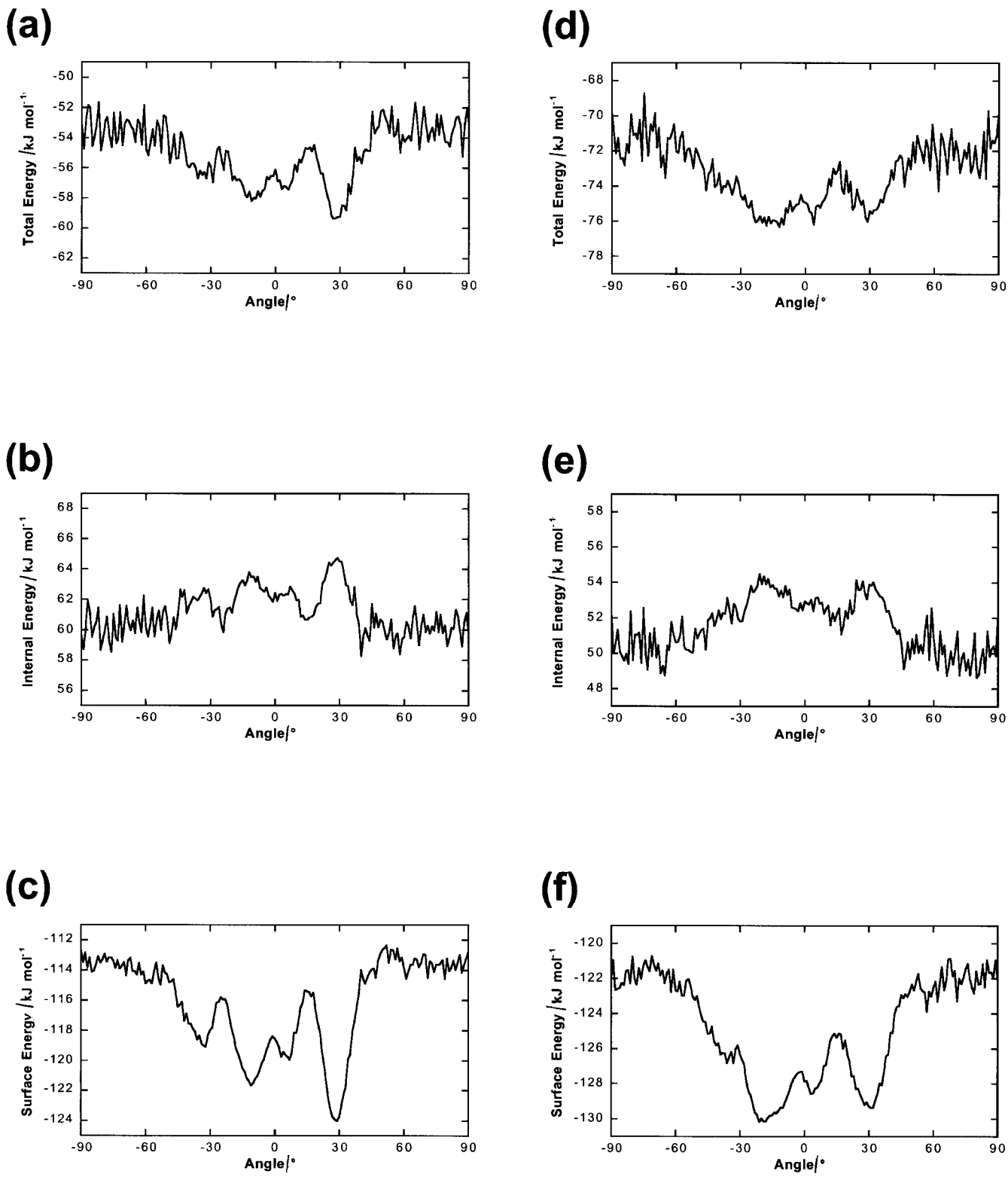

Figure 16. Graphs showing the potential energy of an 8CB molecule on polyethylene crystal surfaces, as a function of the angle of the molecular rigid core. (*a*) The total potential energy of the 8CB molecule on the (1 0 0) surface; (*b*) the corresponding internal energy of the molecule and (*c*) the surface energy term. (*d*) The total potential energy for the (1 1 0) surface; (*e*) the corresponding internal energy and (*f*) the surface energy.

are rather poor approximations to the shape of a real polymer surface.

Further insight into the aligning process may be obtained by examining the average energy of the liquid crystal molecule as a function of the orientation of the core. This is shown in figure 16 for 8CB on the (1 0 0) and (1 1 0) surfaces of PE. By comparing with figure 12, it can be seen that the energy is indeed lowest when the molecule assumes the preferred orientations already identified. However, the internal energy, taken as the sum of the short range non-bonded, bond-stretch, bond-angle and dihedral energy terms is, on average, maximized for these configurations. Thus, the surface interaction energy is dominating the behaviour of the system, and causing the liquid crystal molecule to deform in order to achieve a low overall energy and a close contact with the surface.

The difference in energy between the most preferred orientation and orientations perpendicular to the corrugations ranges between 4 and 6 kJ mol^{-1} for the two surfaces. Since these figures are substantially larger than kT, it is not surprising that orientation of a *single* molecule is possible, and that the influence of neighbouring molecules, for example via a 'nematic field' is not required to overcome thermal fluctuations. On the other hand, the difference in energy between orientations at around 30° to the corrugation axis and orientations approximately parallel to the corrugations is much less, ranging between 0 and 1.5 kJ mol^{-1}. This helps to explain the observation, from previous simulations, that when neighbouring molecules are introduced the preferred orientation switches to being parallel to the substrate chain axis. The energetic requirements of close packing are sufficient to bias the system towards a less favourable surface interaction.

The same effect has been found when using the PE pseudopotential as the basis for simulations of the interfacial region between the alignment surface and the bulk liquid crystal phase [30]. Since it is well known that liquid crystallinity is a co-operative effect, it is clear that simulations containing large numbers of liquid crystal molecules are required in order to study interfacial effects in detail. The pseudopotential approach confers a big advantage for such simulations, because it removes the need to calculate interactions due potentially to thousands of surface atoms. The consequent improvement in simulation speed enables larger systems and longer time scales to be simulated. Work is in hand to exploit this fact in further simulations of this type.

8. Conclusions

We have demonstrated the use of pseudopotentials to represent aligning surfaces in atomistic simulations of liquid crystals at interfaces. We have shown that there are several advantages to the technique. Through the use of generic cosine potential energy functions, we have observed that the degree of orientation achievable increases as the corrugation wavelength decreases and as its amplitude increases. By using different variants of the potential energy function, we have also been able to show that the most important aligning effect is the variation in potential well depth between the peaks and troughs of the corrugations, rather than the topography of the corrugations themselves. Comparisons between the cosine pseudopotentials and the PE pseudopotentials demonstrate that the shape of the corrugation profile is also very important in selecting orientational preferences.

The PE pseudopotential performed well in comparison with previous all-atom simulations. A good agreement was obtained between the preferred orientations of the mesogenic cores of both 8CB and MBF and those found previously. However, the time saving that resulted from using the pseudopotential meant that significantly longer timescales could be explored, with a consequent improvement in the quality of the statistics produced. A study of the separate contributions to the potential energy of the 8CB molecule showed that the molecule deforms in order to achieve a good contact with the pseudopotential surface. The pseudopotential failed to reproduce the alignment behaviour of the flexible tails of the liquid crystal molecules, because the averaging of the surface potential along the substrate chain axis eliminated the possibility of epitaxial alignment. However, the greater mobility of the tails does not appear to influence the aligning behaviour of the rigid cores, and would not appear to be a great disadvantage in the use of the pseudopotential, especially when weighed against the significant reduction in computer time achieved. The pseudopotential will be of benefit in future simulations of the interfacial region between bulk liquid crystal phases and polymer alignment layers.

The authors are grateful to CRL, MSI and the EPSRC for financial support of this project through the provision of a CASE studentship, a computer workstation and access to the Cerius2 simulation package. They also wish to thank Dr Paul Surguy for useful discussions.

References

[1] Chen, W., Feller, M. B., and Shen, Y. R., 1989, *Phys. Rev. Lett.*, **63,** 2665.
[2] Barmentlo, M., van Aerle, N. A. J. M., Hollering, R. W. J., and Damen, J. P. M., 1992, *J. Appl. Phys.*, **71,** 4799.
[3] Foster, J. S., and Frömmer, J. E., 1988, *Nature*, **333,** 542.
[4] Smith, D. P. E., Horber, J. K. H., Binning, G., and Nejoh, H., 1990, *Nature*, **344,** 641.
[5] Iwakabe, Y., Hara, M., Kondo, K., Tochigi, K., Mukoh, A., Yamada, A., Garito, A. F., and Sasabe, H., 1991, *Jpn. J. appl. Phys., 1*, **30,** 2542.

[6] McMaster, T. J., Carr, H. J., Miles, M. J., Cairns, P., and Morris, V. J., 1991, *Liq. Cryst.*, **9,** 11.
[7] Geary, J. M., Goodby, J. W., Kmetz, A. R., and Patel, S. J., 1987, *J. appl. Phys.*, **62,** 4100.
[8] Van Aerle, N. A. J. M., Barmentlo, M., and Hollering, R. W. J., 1993, *J. appl. Phys.*, **74,** 3111.
[9] Wilson, M. R., 1999, *Struct. Bonding*, **94,** 41.
[10] Miyazaki, T., Shigematsu, K., and Yamashita, M., 1998, *J. phys. Soc. Jpn.*, **67,** 3477.
[11] Palermo, V., Biscarini, F., and Zannoni, C., 1998, *Phys. Rev. E*, **57,** R2519.
[12] Gruhn, T., and Schoen, M., 1997, *Phys. Rev. E*, **55,** 2861.
[13] Wall, G. D., and Cleaver, D. J., 1997, *Phys. Rev. E*, **56,** 4306.
[14] Gruhn, T., and Schoen, M., 1998, *J. chem. Phys.*, **108,** 9124.
[15] Stelzer, J., Galatola, P., Barbero, G., and Longa, L., 1997, *Phys. Rev. E*, **55,** 477.
[16] Zhang, Z., Chakrabarti, A., Mouritsen, O. G., and Zuckermann, M. J., 1996, *Phys. Rev. E*, **53,** 2461.
[17] Cleaver, D. J., and Tildesley, D. J., 1994, *Mol. Phys.*, **81,** 781.
[18] Cleaver, D. J., Callaway, M. J., Forester, T., Smith, W., and Tildesley, D. J., 1995, *Mol. Phys.*, **86,** 613.
[19] Yoneya, M., and Iwakabe, Y., 1995, *Liq. Cryst.*, **18,** 45.
[20] Yoneya, M., and Iwakabe, Y., 1996, *Liq. Cryst.*, **21,** 347.
[21] Yoneya, M., and Iwakabe, Y., 1996, *Liq. Cryst.*, **21,** 817.
[22] Doerr, T. P., and Taylor, P. L., 1999, *Int. J. Mod. Phys. C*, **10,** 415.
[23] Doerr, T. P., and Taylor, P. L., 1999, *Mol. Cryst. liq. Cryst.*, **330,** 1735.
[24] Patnaik, S. S., and Pachter, R., 1999, *Polymer*, **40,** 6507.
[25] Binger, D. R., and Hanna, S., 1997, *Mol. Cryst. liq. Cryst.*, **302,** 63.
[26] Binger, D. R., and Hanna, S., 1999, *Liq. Cryst.*, **26,** 1205.
[27] Binger, D. R., and Hanna, S., 2000, *Liq. Cryst.*, **27,** 89.
[28] Billmeyer Jr., F. W., 1984, *Textbook of Polymer Science*, 3rd. Edn (New York: Wiley).
[29] Myrvold, B. O., 1993, *Abs. Pap. Am. chem. Soc.*, **205,** 372-POLY.
[30] Binger, D. R., and Hanna, S. (in preparation).
[31] Steele, W. A., 1973, *Surf. Sci.*, **36,** 317.
[32] Talbot, J., Tildesley, D. J., and Steele, W. A., 1984, *Mol. Phys.*, **51,** 1331.
[33] Joshi, Y. P., and Tildesley, D. J., 1985, *Mol. Phys.*, **55,** 999.
[34] Bunn, C. W., 1939, *Trans. Faraday Soc.*, **35,** 482.
[35] Mayo, S. L., Olafson, B. D., and Goddard, W. A., 1990, *J. phys. Chem.*, **94,** 8897.
[36] Leach, A. R., 1996, *Molecular Modelling Principles and Applications* (Harlow, England: Addison Wesley Longman), p. 177.
[37] Chandrasekhar, S., 1992, *Liquid Crystals*, 2nd. Edn (Cambridge: Cambridge University Press).
[38] Gray, G. W., Harrison, K. J., Nash, J. A., Constant, J., Hulme, D. S., Kirton, J., and Raynes, E. P., 1974, in *Liquid Crystals and Ordered Fluids*, Vol. 2, edited by J. F. Johnson and R. S. Porter (London: Plenum), p. 617.
[39] Leadbetter, A. J., Durrant, J. L. A., and Rugman, M., 1977, *Mol. Cryst. liq. Cryst.*, **34,** 231.
[40] Gray, G. W., Harrison, K. J., and Nash, J.A ., 1975, *Pramana Suppl.*, **1,** 381.
[41] Forester, T. R., and Smith, W., 1995, *DL_POLY molecular dynamics code*, CCP5 of the EPSRC.
[42] Cerius2 v.3.5, Molecular Modelling Software, available from Molecular Simulations Ltd., 240/250 The Quorum, Barnwell Road, Cambridge CB5 8RE, U.K. (http://www.msi.com/).
[43] Binger, D. R., 1997, PhD thesis, University of Bristol, UK
[44] Berreman, D. W., 1973, *Mol. Cryst. liq. Cryst.*, **23,** 215.